Divergent convective outflow in large eddy simulations, supplementary material

Edward Groot[1] and Holger Tost[1]

[1]Institut für Physik der Atmosphäre, Johannes Gutenberg Universität, Johannes-Joachim-Becher-Weg 21, Mainz, Germany

Correspondence: Edward Groot (egroot@uni-mainz.de)

1 Initial potential temperature profile shape used for finite length squall lines

The shape of potential temperature perturbations along the y-axis is shown in Figure S1.

2 Accumulated precipitation

In Figure S2 one can see the mean precipitation accumulation for each mode of convection, as well as the ensemble spread for some thresholds of cumulative precipitation. It is shown for the background ensemble and the perturbed convective momentum transport simulations. The latter set is shown, because the area of precipitation accumuluation is generally displaced or deformed the most within these experiments compared to the reference simulation (which itself is included in the "spaghetti" plots). Other perturbations introduce weak(er) displacements. Furthermore, perturbed latent heating in particular affects mostly the amplitude of the precipitation signals.

The figure shows that the latent heating is injected in the column within a rather compact region: in particular for the regular multicell (second from the left). The ensemble spread is narrow. The precipitation cells also occur in a condensed area during the two hours simulation time in simulations with physics perturbations. Furthermore, the high degree of symmetry along the length of the infinite length squall line stands out (third from the left, top and bottom).

A compact and persistent region of high precipitation accumulation was intended and is achieved.

3 Mid-level vertical motion

A selection of panels with the evolution of mid-level and near-tropopause vertical velocity in the control simulation of the four modes of convection is presented here. In Figure S3 the vertical velocity in the middle troposphere is shown. After 25 minutes of simulation time the gravity wave signal that propagates away from the convective cells (which are white) is represented by an outer ring of subsidence in the supercell and the regular multicell simulations. That ring is still restricted to a very small region within 20 km (10 km) of the convective core (close to the origin). In both of the squall line simulations, the convection develops a little bit quicker and the subsidence ring has already grown further, reaching more than 30 km outward from main

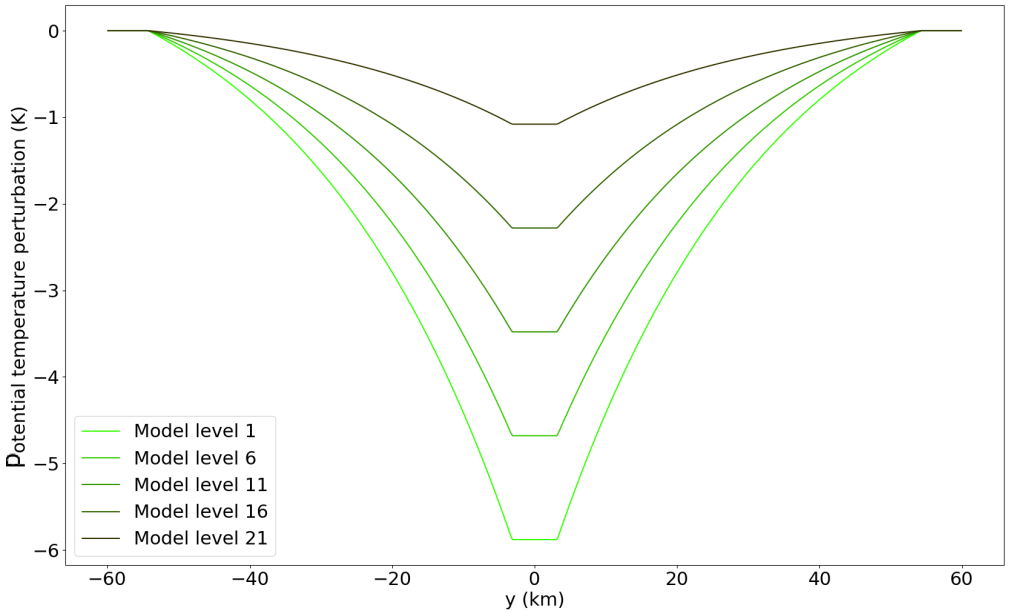

Figure S1. North-south profile of initial potential temperature perturbations along the length of the finite length squall line for five selected model levels, counted upward from the surface level.

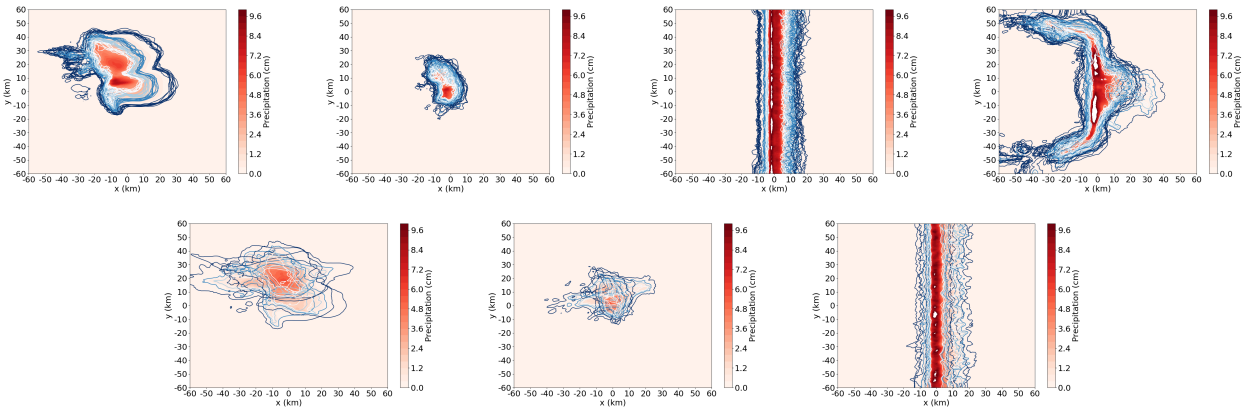

Figure S2. Mean precipitation accumulation (red color scale) and isolines for 1, 10, 20 and 30 mm (blue-white). Top: ensemble spaghetti plots for (left) supercell; (left center) regular multicell; (right center) infinite length squall line; (right) finite length squall line. Bottom: same, for perturbed convective momentum transport. (On the left) supercell; (center) regular multicell; (right) infinite length squall line.

convective line. Such a ring of subsidence has been documented regularly in literature (Bretherton and Smolarkiewicz (1989); Mapes (1993) and by many after them, e.g. Bierdel et al. (2017)). This is a response and compensation to the upward mass transport that the convection governs onto its environment.

Looking at w after 50 minutes (Figure S3) subsequent gravity wave signals partially lead to upward motion in the middle troposphere. On the left in the supercell case, the signal is clearly much stronger in the direction along the wind shear than in the meridional direction, perpendicular to the wind shear. Substantial gravity wave activity occurs in the 20-40 km east of the supercell, where higher frequency gravity waves are superposed onto one another. Upstream of the supercell the motion is still downward.

The signal associated with the regular multicell is still largely circular, with alternating upward and downward motion. Looking at the infinite squall line, a lot of upward motion in the middle troposphere occurs, which has propagated slightly further upstream than downstream to an area covering a range up to about 40 km away from the y-axis. However, the wavelengths are relatively long (still). In case of the finite squall line, the pattern is similar to the infinite squall line, but the area covered is comparatively reduced, up to 30 km from the y-axis.

In the last panel (90 and 75 minutes), waves with shorter length also spread out substantially: for the supercell case, about half of the area in the northeastern corner is dominated by the shortwave signal. The assymmetric propagation occurs due to the strong westerly upper tropospheric flow, leading to a mean wind that is also eastward. However, the convective cores remain near the center.

The shorter wavelength signals for the regular multicell still stick to a portion of the domain within about 30-40 km radius from the convective cores. The convective cells also nicely stick to the center. Similarly, weak (slightly eastward) propagation of the infinite squall line has occurred. Associated shortwave gravity waves have occupied more or less the whole domain by now, as opposed to the finite squall line, where most effects are restricted to a region up to about 40 km from the y-axis and the southern most 10 km of the domain also does not show strong gravity wave signals. Exception to the latter is the first local signal from newly initiated convective cells at the southwestern corner of the domain.

4 Extra panels, Figure 4 (main text)

Figure S4 shows an extended version of Figure 4 in the main text. It shows how (in)appropriate outflow integration masks at 7-14 km are: for some -40% latent heating simulations (left column, lowest outflow levels) the divergent outflow is generally located at 6-11km altitude instead.

5 Separate u- and v- components of divergence in infinite and finite length squall line simulations

The existence of two regimes (2D and 3D divergence) has been suggested in the previous section and by linear gravity wave models forced by heating as discussed in earlier literature (Bretherton and Smolarkiewicz, 1989; Nicholls et al., 1991; Mapes, 1993; Pandya and Durran, 1996; Nascimento and Droegemeier, 2006). In this section the u- and v-component of the upper

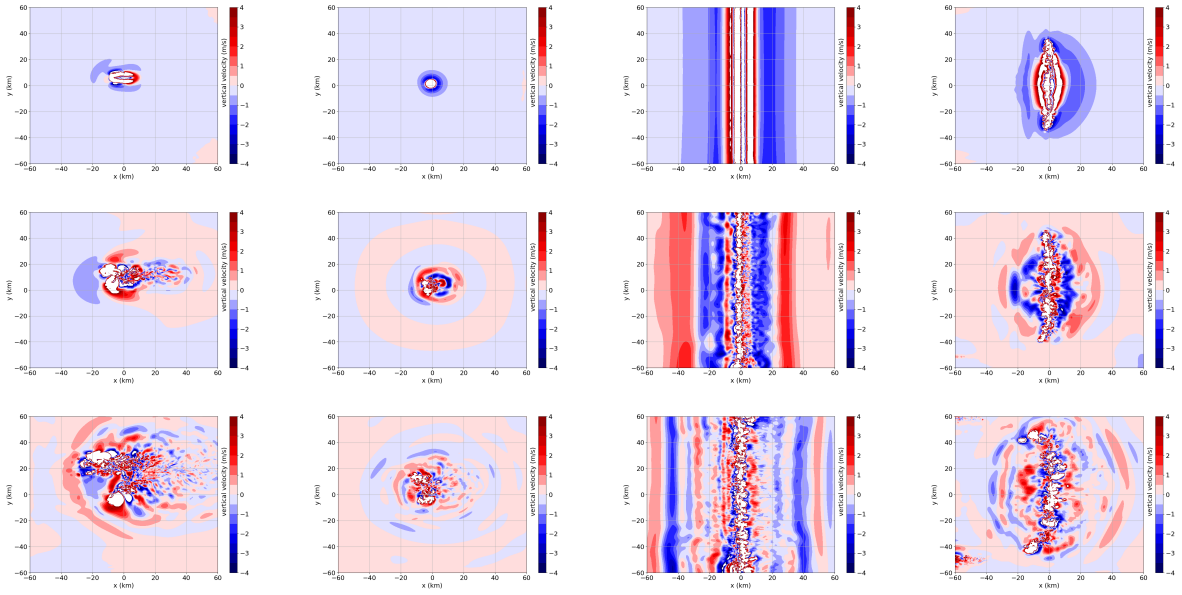

Figure S3. w at 6 km height for the control simulations. Left column: supercell; center: regular multicell; right: squall line. From top to bottom row: 25 min (top), 50 min (center) and 90/90/75/75 min (bottom row). The cell cores appear in white, as they (largely) exceed ± 4 m/s.

tropospheric divergence are separately investigated for the finite length squall line.

Figure S5 shows that during the initial time interval, the meridional divergence is negligible throughout most of the domain. The only small contributions by the v-term arise at the end points of the squall line, the northern and southern edge. Similar patterns have been identified for the infinite length squall line, but without the presence of the squall line end in case of an infinite length squall line. All divergence occurs initially in the u-component, which is consistent with the existence of a 2D regime and a 3D regime. During the second time interval, the v-components develop particularly strongly on the northern and southern arching regions of the squall line. Both components are of the same order of magnitude, but that is expected for a strongly curved squall line (as indicated by precipitation accumulation).

The divergence in Figure S5a is about an order of magnitude larger than in Figure S5b in the squall line centre. This is also consistent with the infinite length squall line, where the difference was about one order of magnitude too. Therefore, the leading order divergence variability in Figure 5 (Main text) can confidently be attributed to the dimensionality of outflows (2D/3D) and associated with that the presence of a pulse or line source of latent heating.

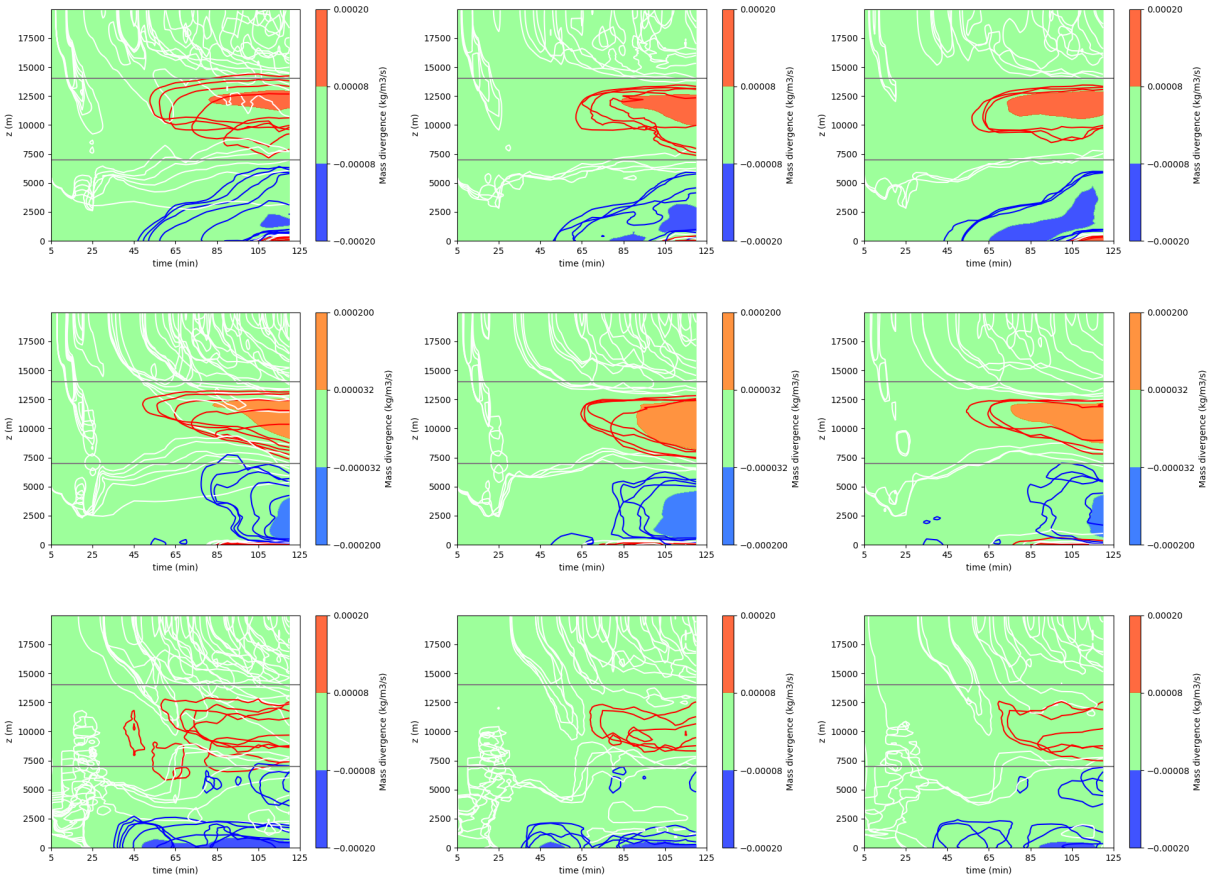

Figure S4. Divergence profiles as in Figure 4 of main text, with mean of the experiments as shading and spaghetti contours for individual experiments, at (blue) -5e-5 kg/m3/s, (white) 0 kg/m3/s and (red) +5e-5 kg (middle column $\pm 2e-5$ kg/m3/s instead). Top to bottom: supercell, regular multicell, infinite length squall line; left to right: latent heating perturbations (-40%, -20%, -10%, +10%, +20%), vertical advection of horizontal momentum (-100%, -50%, +50%) and near-surface potential temperature perturbations.

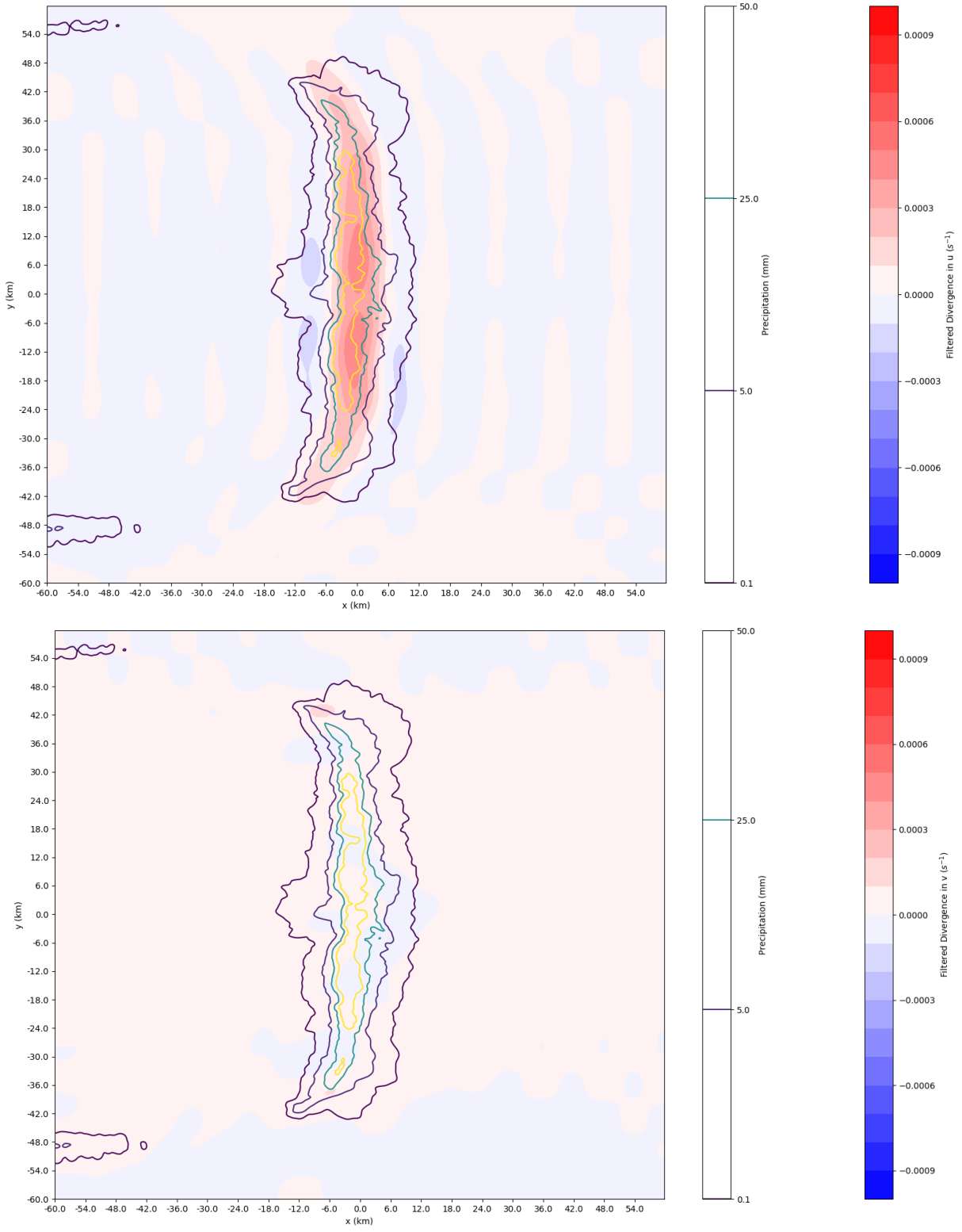

Figure S5. Filtered divergence over altitudes 7-14 km for a finite squall line duringfirst time interval. Wavelengths that fit more than 20 times in the domain have been removed with a discrete Fourier transform. Contours indicate the accumulated precipitation pattern during each of the two time intervals. Zonal component (left) and meridional component (right).

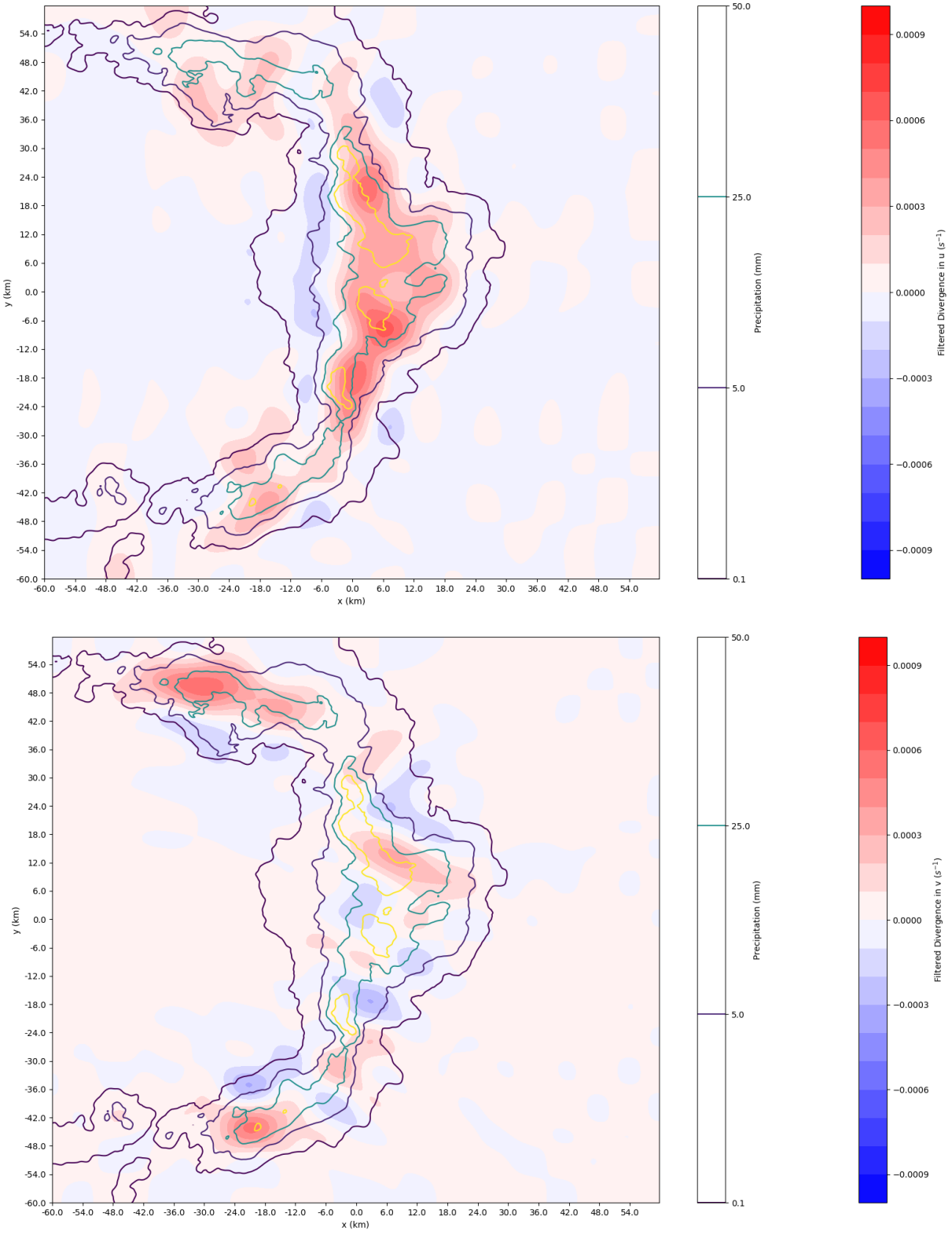

Figure S6. Filtered divergence over altitudes 7-14 km for a finite squall line during second time interval. Wavelengths that fit more than 20 times in the domain have been removed with a discrete Fourier transform. Contours indicate the accumulated precipitation pattern during each of the two time intervals. Zonal component (left) and meridional component (right).

References

Bierdel, L., Selz, T., and Craig, G.: Theoretical aspects of upscale error growth through the mesoscales: an analytical model, Quarterly Journal of the Royal Meteorological Society, 143, 3048–3059, https://doi.org/10.1002/qj.3160, https://doi.org/10.1002/qj.3160, 2017.

Bretherton, C. S. and Smolarkiewicz, P. K.: Gravity Waves, Compensating Subsidence and Detrainment around Cumulus Clouds, Journal of Atmospheric Sciences, 46, 740 – 759, https://doi.org/10.1175/1520-0469(1989)046<0740:GWCSAD>2.0.CO;2, https://journals.ametsoc.org/view/journals/atsc/46/6/1520-0469_1989_046_0740_gwcsad_2_0_co_2.xml, 1989.

Mapes, B. E.: Gregarious Tropical Convection, Journal of Atmospheric Sciences, 50, 2026 – 2037, https://doi.org/10.1175/1520-0469(1993)050<2026:GTC>2.0.CO;2, https://journals.ametsoc.org/view/journals/atsc/50/13/1520-0469_1993_050_2026_gtc_2_0_co_2.xml, 1993.

Nascimento, E. L. and Droegemeier, K. K.: Dynamic Adjustment in a Numerically Simulated Mesoscale Convective System: Impact of the Velocity Field, Journal of the Atmospheric Sciences, 63, 2246 – 2268, https://doi.org/10.1175/JAS3744.1, https://journals.ametsoc.org/view/journals/atsc/63/9/jas3744.1.xml, 2006.

Nicholls, M. E., Pielke, R. A., and Cotton, W. R.: Thermally Forced Gravity Waves in an Atmosphere at Rest, Journal of Atmospheric Sciences, 48, 1869 – 1884, https://doi.org/10.1175/1520-0469(1991)048<1869:TFGWIA>2.0.CO;2, https://journals.ametsoc.org/view/journals/atsc/48/16/1520-0469_1991_048_1869_tfgwia_2_0_co_2.xml, 1991.

Pandya, R. E. and Durran, D. R.: The influence of convectively generated thermal forcing on the mesoscale circulation around squall lines, Journal of the Atmospheric Sciences, 53, 2924–2951, https://doi.org/10.1175/1520-0469(1996)053lt;2924:tiocgtgt;2.0.co;2, 1996.